J Mater Sci (2022) 57:8987–9001

Polymers & biopolymers

Fabrication of hydrophobic PLA filaments for additive manufacturing

Rajakaruna A. D. N. V. Rajakaruna[1], Balakrishnan Subeshan[1], and Eylem Asmatulu[1,*]

[1] *Department of Mechanical Engineering, Wichita State University, Wichita, KS 67260, USA*

Received: 22 February 2022
Accepted: 9 April 2022
Published online: 29 April 2022

ABSTRACT

There is an ever-greater need for self-cleaning and water-repelling properties of hydrophobic materials at this time in history, mainly due to the coronavirus disease 2019 (COVID-19) pandemic. However, the fabrication processes used to create hydrophobic materials are typically time-consuming and costly. Thus, this study aims to create hydrophobic materials based on low-cost manufacturing. In this study, polylactic acid (PLA) was mixed with various concentrations of hexadecyltrimethoxysilane (HDTMS) and polytetrafluoroethylene (PTFE) with the aid of solvents, chloroform, and acetone, through the solvent casting and melt extrusion process, which is capable of producing hydrophobic PLA filaments suitable for additive manufacturing (AM). Water contact angle (WCA) measurements were performed to verify the improved hydrophobicity of PLA/HDTMS/PTFE filaments. According to the results, it was discovered that the best filament WCAs were achieved with 2 g (10 wt%) of PLA, 0.2 ml of HDTMS, and 1 ml of PTFE (2 g PLA + 0.2 ml HDTMS + 1 ml PTFE), producing an average WCA of 131.6° and the highest WCA of 132.7°. These results indicate that adding HDTMS and PTFE to PLA significantly enhances filament hydrophobicity. Additionally, scanning electron microscopy (SEM), Fourier transform infrared spectroscopy (FTIR), and thermogravimetric analysis (TGA) techniques were utilized to characterize the surface morphology, molecular interactions, and thermal decompositions of the prepared PLA/HDTMS/PTFE filaments. This study revealed that compared to 2 g of pure PLA filament, HDTMS and PTFE altered the microstructure of the filament. Its thermal degradation temperature was impacted, but the melting temperature was not. Therefore, the PLA/HDTMS/PTFE filament is good enough to be printed by the fused filament fabrication (FFF) AM process.

Handling Editor: Maude Jimenez.

Address correspondence to E-mail: e.asmatulu@wichita.edu

https://doi.org/10.1007/s10853-022-07217-5

GRAPHICAL ABSTRACT

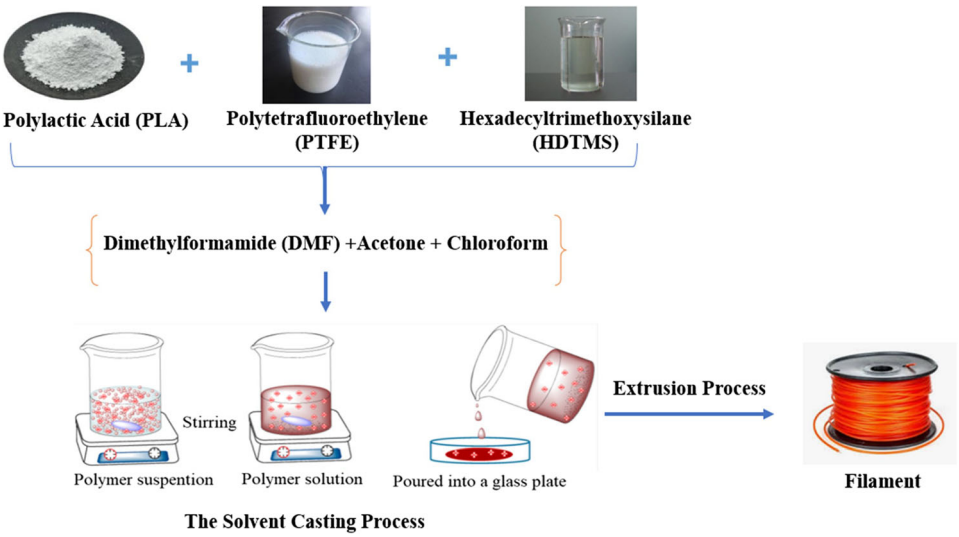

Introduction

Hydrophobic properties were observed in nature before human beings discovered their true capabilities and utilized them to revolutionize the modern world. The most familiar form of hydrophobicity found in nature is that of the lotus leaf, where its self-cleaning and water-repelling properties make it one of the best hydrophobic elements formed naturally [1, 2]. Since its discovery, artificially created hydrophobic materials have been used in many industries, including automobile [3], aerospace [4], medical [5], and maritime [6]. Moreover, surface hydrophobicity mainly depends on its roughness and its chemistry—the greater the surface roughness, the greater the hydrophobicity [7, 8]. The management of the hydrophobicity of solid surfaces is crucial for many industrial applications. A surface's hydrophobicity can be measured by depositing a water droplet on a surface and determining the water contact angle (WCA) that it creates [9]. A surface is known to be hydrophobic if it has a WCA between 90° and 150° when it comes in contact with a liquid droplet. On these water surfaces, the liquid droplet appears almost round in shape due to the increased wetting resistance, thus preventing the droplet from dispersing once meeting the surface [10].

With the development of nanotechnology, hydrophobic surfaces have attracted considerable attention. Hierarchical micro- and nanoscale roughness on a surface traps air there and increases the WCA [11]. Moreover, low surface energy decreases the tendency of water to bond with the surface. With this understanding, scientists have designed different types of micro-nano-hydrophobic materials [12]. Hydrophobic surfaces can be developed through chemical [13], electrochemical [14], and physical surface treatments [15], thereby increasing surface roughness [16] or forming a surface coating [17]. To achieve nanoscale roughness on a hydrophobic surface, different techniques such as polymer solution evaporation [18], sol–gel coating [19], electrochemical deposition [20], photolithography [21], chemical etching [22], phase separation [23], self-assembly [24], and various spraying techniques are used [25, 26]. However, these techniques for preparing hydrophobic surfaces are difficult and expensive. They can also be categorized according to direction: top-down, bottom-up, or both. The lithographic process, template-based techniques, and plasma treatment operate top-down, while the chemical deposition, layer-

by-layer, and hydrogen bonding methods operate bottom-up [27, 28]. Furthermore, the casting of polymer solutions and phase separation techniques use a combination of both top-down and bottom-up methods. Finally, all fabrication methods utilize hydrophobic material (e.g., silicone, polypropylene, carbon nanotube), hydrophobic modifying agents (e.g., fluoroalkyl-silane, alkyl-thiol, alkyl-dicarboxylic acid), and active substrates (e.g., polymer, metal, metallic oxide) [29–31].

Over the years, many studies have been carried out to determine how materials increase surface hydrophobicity. Morita et al. determined that the particle size of PTFE and temperature had desirable effects on the hydrophobicity of a surface. Carbone et al. modified the surface of PTFE using plain argon (Ar) and an argon/oxygen (Ar/O_2) plasma formed using a torch with an atmospheric-pressure radio frequency, achieving a WCA of 130°[32]. Various other substances could be added to PLA to obtain greater hydrophobicity. Ryu et al. succeeded in raising the hydrophobicity of PLA by mixing it with HDTMS-modified zinc oxide (ZnO). They created a nanocomposite comprising PLA and HDTMS-modified ZnO by adding the HDTMS-modified ZnO into the PLA matrix fabricated through the solvent casting process. According to the structural analysis of the nanoparticles, it was observed that ZnO was successfully modified and that the modification influenced both the dispersibility and hydrophobicity of the samples [33]. Shaker et al. conducted an experiment to enhance the hydrophobicity of stainless steel by mixing it with sol–gel-based alumina and HDTMS. The sample was then sintered at a temperature of 900 °C to obtain a hydrophobic surface, the result of micro-/nanoscale cracking, aggregations, and particle-coarsening at a temperature of 900 °C, which gave rise to the hydrophobic surface. According to results, a WCA as high as 132° was recorded, thus proving hydrophobicity [34].

The demand for self-cleaning and water-repellent properties is now higher than ever due to the coronavirus disease 2019 (COVID-19) pandemic. Ever since discovering the capability of the COVID-19 virus to remain on surfaces for days, scientists around the world have been working to create products that can clean themselves, thereby preventing contamination by the COVID-19 virus [35]. This could be enormously beneficial to health workers and other essential workers. Personal protective equipment (PPE) such as face masks, head coverings, hazmat suits, boots, and customized medical devices is necessary for frontline health care workers, various industry workers, and ordinary human beings who face contamination in their daily lives [36]. This PPE is now being manufactured using hydrophobic materials and tested for better self-cleaning and water-repellency capabilities. One of the techniques used in the contemporary world to create PPE is additive manufacturing (AM).

AM offers a cheaper and faster technique than traditional subtractive manufacturing to produce products with complex shapes [37–39]. In recent years, AM has gained popularity for the direct manufacturing of complex geometrical objects, which enables the production of high-quality products without using a template tool and thereby reducing waste. A further advantage of AM over traditional subtractive manufacturing techniques is the possibility of reducing waste materials by up to 90% during the production process. Because of these advantages, this technique has emerged as a viable alternative to traditional manufacturing methods for aerospace, automobile, healthcare, and consumer goods [40, 41]. 3D printed hydrophobic surfaces have found many applications in industry including anti-fog surface, anti-freeze surfaces for aircrafts, self-cleaning surfaces for everyday life, agriculture, industry, and military industries, oil and water separation, anti-bacterial surfaces, drag reduction surface for aircraft, submarines, and shipping equipment, sensor and battery manufacturing, desalination water purification medical applications, liquid flow and penetration control which is highly important in microfluidic devices. Up to now, many 3D printed hydrophobic surfaces with proposed applications have been fabricated by AM. There is the possibility for PPE to be manufactured from thermoplastics without compromising any of its integrity or functionality. Although AM can be used to produce PPE by combining thermoplastics, such as polylactic acid (PLA), polyvinyl ether (PVE), and polythene (PE), there are practical challenges associated with handling this kind of material [42].

Unfortunately, the current potential for AM is hindered by the limited choice of materials that meet necessary performance specifications for a particular application. Thermoplastics are often used for AM applications, so they are typically the primary material source for customer-level AM systems. [43].

Additionally, they are easily incorporated into AM applications and are capable of being produced using different techniques, such as selective laser melting (SLM) [44], powder bed fusion (PBF) [45], stereolithography (SLA) [46], material jetting (MJ) [47] and fused filament fabrication (FFF) [48]. FFF is an excellent method for printing thermoplastics and is one of the most popular and cost-effective AM techniques. Enabling filaments to have their own self-cleaning and water-repellent properties for additively manufactured parts is essential to minimizing the risk of material shortages during their use. [49–51].

AM is rapidly gaining popularity in the manufacturing world due to its low cost, easy accessibility, modifiable design and testing. As the name implies, AM refers to the process of adding materials layer by layer to a structure, following a computer-aided design (CAD) model [52]. A 3D design is initially created using CAD software to create a model through AM. Later, information for the object is transferred to an AM printer through digital slicing of the CAD design. The AM equipment then produces a 3D object depending on the machine's technology. It has been a decade since AM technologies have evolved into fused filament fabrication AM technology, which is now the most widely used AM method due to its reliability, simplicity, affordability, and minimal waste generation. FFF involves the extrusion of filament, a thermoplastic material, through an extrusion nozzle using a filament-feeding roller [53, 54].

PLA, a widely used thermoplastic in FFF, is a semi-crystalline or amorphous polymer. It has a melting temperature of 180 °C and an approximate glass transition temperature (T_g) of 55 °C. Moreover, PLA is highly insoluble in liquids such as water and common alcohols like ethanol, yet soluble in organic solvents such as chloroform and dichloromethane [55]. Therefore, in many applications, it is necessary to modify PLA in order to enhance its mechanical and thermal properties. As more people become aware that traditional thermoplastics generated from petrochemicals can accumulate in the environment and cause long-term harm, efforts have been made to develop and market replacement thermoplastic polymers that are more amenable to recycling [56, 57]. Another polymer, employed in this study, is PTFE, a fluoropolymer of tetrafluoroethylene, commonly known as Teflon™. PTFE is a compact and rigid polymer with excellent thermal stability owing to its linear arrangement and absence of branching [58].

Although there have been recent advancements in FFF, a lack of feedstock polymers has proven to be a barrier to its expansion and further development [59]. Furthermore, there are also certain disadvantages of using the current pure polymeric materials for FFF, including high cost, low strength, and easy distortion, which limit their use in cost-efficient, functional, and load-bearing applications and large-scale production [60–63]. Thus, the development of new FFF filaments is an essential topic within the additive manufacturing field. The novelty of the study was to fabricate and characterize a polymer-filled PLA filament used for the FFF AM process featuring an exceptional hydrophobic surface with self-cleaning and water-repellent properties. The polymer-filled PLA filament was fabricated with the addition of HDTMS and PTFE in PLA with the aid of solvents. The prepared solution was cast and subsequently extruded to form filaments for the FFF AM process, which enhanced hydrophobicity to prevent contamination.

Materials and methods

Materials

For the present study, PLA powder with an average particle size of 325 µm and a melting temperature of 150–170 °C was obtained from Making Cosmetics Inc. HDTMS was obtained from Sigma-Aldrich and chloroform from Sisco Research Laboratories, both used without further purification. A PTFE solution with a particle size of 3 µm and acetone were obtained from the Sri Lanka Institute of Nanotechnology (SLINTEC).

Methods

The filaments for this study were created by adding a solution of HDTMS and PTFE into PLA at various concentrations and then solvent casting them. First, 2 g (10 wt%) of PLA only was dissolved in 12 ml of chloroform and sonicated in an ultrasound probe sonicator at 20 kHz of frequency and 750 W, with pulses of 20 s with 5 s at rest for 30 min.; then, 8 ml of acetone was slowly added to the solution and

sonicated for another 30 min. Next, 0.2 ml of HDTMS was slowly added to the solution, and the system was kept sealed and stirred at 770 rpm for 30 min. on a hot plate until a complete homogenous solution was formed. Then, 1 ml of PTFE solution was added to the solution and stirred for 30 min at 40 °C on the hot plate. Afterward, the 2 g PLA + 0.2 ml HDTMS + 1 ml PTFE solution was poured into a Petri dish for solvent casting. In order to evaporate the solvent, the samples were kept in a fume hood for approximately 24 h. at ambient temperature. Furthermore, the samples were dried in an industrial oven at 60 °C for approximately 4 h. to remove any residual solvent or moisture.

Another sample was prepared by increasing the PTFE concentration from 1 to 2 ml and solvent casting it while keeping the other concentrations constant. Three additional sets of samples were prepared using the same procedure. One sample was created by dissolving 2 g (10 wt%) of PLA only in 12 ml of chloroform and 8 ml of acetone, while another sample was formed by adding 0.4 ml of HDTMS to the solution with similar concentrations of PLA, chloroform, and acetone as for the first sample. After adjusting the concentration of HDTMS to 0.8 ml, the final sample was prepared. All prepared highly concentrated samples were then solvent cast, kept in a fume hood for drying for approximately 24 h. at ambient temperature, and subsequently kept in an industrial oven for drying at a temperature of 60 °C for approximately 4 h. The solvent-cast PLA/ HDTMS/ PTFE samples exhibited sufficient malleability, in order to be ground into small flakes after evaporating the excess chloroform and acetone.

The filament fabrication process was performed using a Filabot EX2 extruder. Here, the solvent-cast PLA/HDTMS/PTFE samples were ground into small pieces and dropped into the extruder feeder. The extruder temperature was set to 190 °C, and then, the process was carried out. After 15 min., the temperature was lowered to 140 °C, and as the polymer melt was extruded, it passed through spinnerets with 0.128 in.-diameter die exits. The PLA/HDTMS/PTFE filaments were fabricated to fit the drive wheels of the FFF AM machines with a consistent diameter in order to ensure smooth operation. The extrudate from the die exit was quenched in 40 mm of water placed in the exit hole of the die. As gravity pulled the filaments into the water, they cooled and hardened, making them more suitable for creating PLA/HDTMS/PTFE filaments. Figure 1 illustrates a schematic illustration of the preparation process used to fabricate these filaments.

Since the cross section of the PLA/HDTMS/PTFE filaments is circular, determining the WCA is highly difficult. Therefore, alternative experimental approach was used to validate the hydrophobicity to characterize the prepared PLA/HDTMS/PTFE filaments. Instead of using extruded PLA/HDTMS/ PTFE filaments, the cast PLA/HDTMS/PTFE samples had been justifiably modified to have the same properties as extruded PLA/HDTMS/PTFE filaments. As part of the justification for the PLA/ HDTMS/PTFE filaments, cast PLA/HDTMS/PTFE samples were prepared according to the same initial procedures of the PLA/HDTMS/PTFE filament as described in this text. However, rather than grinding the cast PLA/HDTMS/PTFE samples, they were heated up to 190 °C for one hr. in an industrial oven. After an hour later, the cast PLA/HDTMS/PTFE solid samples began to melt. After the melting process, the cast PLA/HDTMS/PTFE samples were flattened and allowed to dry for 24 h. at room temperature prior to the surface hydrophobicity studies. The smooth flatten surfaces were used for the WCA tests with the high accuracy. Four measurements were conducted on each sample, and the test results were averaged for each data point since the WCA values were minimum. Based on our initial experiments, the range between the WCA values of extrusion and quenching results was usually within 5–10%, so we neglected that part of the study. From this point forward, the flattened sample was referred to as PLA/HDTMS/PTFE filament and was used for further WCA measurements and characterization studies.

The wettability of a surface is an essential characteristic of hydrophobic materials. The wettability of all prepared filaments was evaluated by measuring the WCA of distilled water drops on the surface of the filaments using a contact angle goniometer. These measurements were conducted at ambient temperature using micro-syringes to deposit drops of water on the PLA/HDTMS/PTFE filaments. The WCA values were determined by averaging five measurements on each prepared filament. Detailed images of the drop on the surface were acquired after 20 s. The surface morphology of the PLA/HDTMS/PTFE filaments was examined with a Hitachi SU6600 scanning electron microscope and a tungsten filament

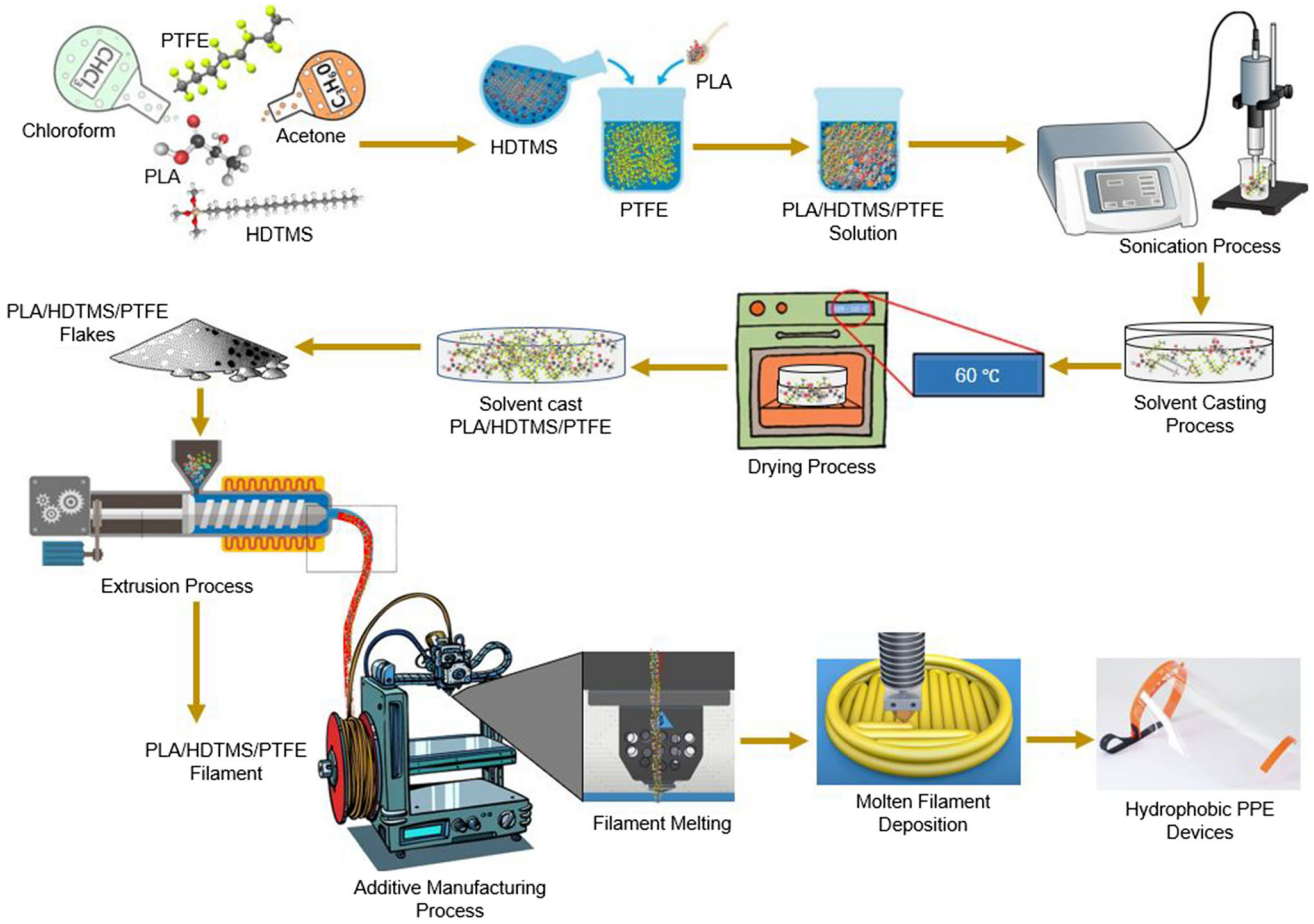

Figure 1 Schematic of preparation process used to fabricate PLA/HDTMS/PTFE filaments for additive manufacturing.

operating at 10 kV using a low vacuum technique at 10 mm. Before the scanning electron microscopy (SEM) analysis, all filaments were coated with a thin layer of gold in order to make them conductive.

The Fourier transform infrared spectroscopy (FTIR) analysis confirmed the identification of functional groups of PLA/HDTMS/PTFE filaments. Specifically, the filaments were scanned into absorbance mode between 4000 and 550 cm^{-1} (wavenumbers) on a Bruker Vertex 80 FTIR spectrometer using a peak attenuated total reflectance (ATR) cell. The thermogravimetric analysis (TGA) was performed with an SDT Q600 thermographic instrument under a nitrogen atmosphere by heating at 10 °C/min and cooling at 30 °C/min. The first heating was done to remove the thermal history of the filament (0 °C to 220 °C). The temperature and enthalpy of fusion and crystallization were calculated using the maximum and peak areas of the second heating curve, respectively.

Results and discussion

Visual representation

The visual representation of the prepared filaments, for the 2 g PLA + 0.2 ml HDTMS + 1 ml PTFE, does not show aggregation, due to the homogenous solution, indicating that the method used to mix PLA, PTFE, and HDTMS resulted in a homogeneous mixture. The homogeneous solution was dried for approximately 24 h. at ambient temperature, after which a white-colored, waxy solid structure was observed, as shown in Fig. 2a. The samples were kept at a temperature of 60 °C for approximately 4 h., which produced a rough solid structure, as shown in Fig. 2b. These solid samples were ground into small flakes, as shown in Fig. 2c, and inserted into the feeder of an extruder. Finally, Fig. 2d shows the PLA/HDTMS/PTFE filament.

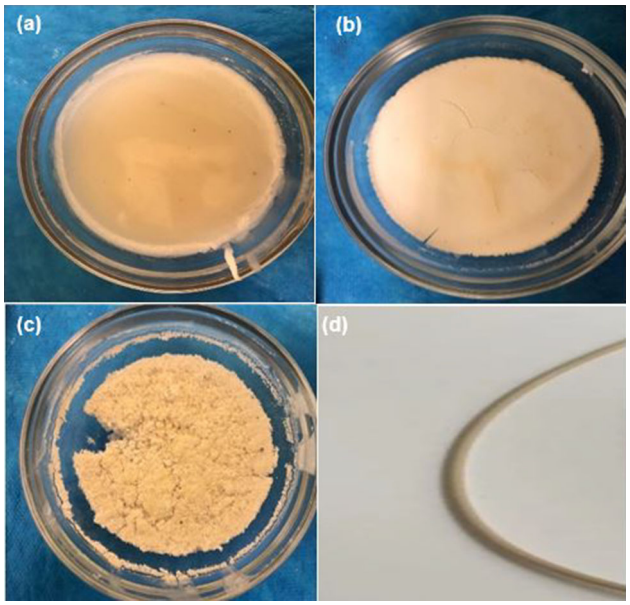

Figure 2 Visual representation images of prepared 2 g PLA + 0.2 ml HDTMS + 1 ml PTFE: **a** after 24 h. drying showing white-colored, waxy solid structure; **b** after 4 h. drying at temperature of 60 °C, showing rough solid structure; **c** after grinding into small flakes; and **d** filament obtained after extrusion.

WCA measurement analysis

The surface wettability of the prepared PLA/HDTMS/PTFE filaments was evaluated according to the composition of polymers in the filaments. The WCA measurements on the prepared filaments' surfaces are presented in Fig. 3. It was found that the 2 g PLA + 0.2 ml HDTMS + 1 ml PTFE filament had a higher WCA than the other filaments under the same conditions. The WCA for 2 g PLA + 0.2 ml HDTMS + 1 ml PTFE filament was 131.6°, whereas the highest value achieved was 132.7°. It was concluded that an increase in hydrophobicity had been achieved based on the results. The reason for the greater WCA observed in the 2 g PLA + 0.2 ml HDTMS + 1 ml PTFE filament could be due to its morphology.

As a result of fewer cavities in the 2 g PLA + 0.2 ml HDTMS + 1 ml PTFE filament, the WCA values were higher and found to be ~ 130°. However, the occurrence of this feature was predictable since the intrinsic roughness of surfaces enhances their hydrophobicity. Furthermore, it may also be caused by the presence of HDTMS. This molecule contains a long-chain structure [64]. As a result, the silicon atoms present could create covalent bonds with the carbon atoms in PLA on the 2 g PLA + 0.2 ml HDTMS + 1 ml PTFE filament to form long chains above the surface, thereby inhibiting the formation of HF bonds between PLA and PTFE and in turn increasing hydrophobicity [65]. After obtaining the WCAs of the prepared PLA/HDTMS/PTFE filaments, it was determined that increasing the PTFE concentration did not increase the hydrophobicity of the filament. Accordingly, the HDTMS concentration was increased, while PTFE concentration remained unchanged. WCA measurements of all prepared PLA/HDTMS/PTFE filaments are shown in Fig. 3.

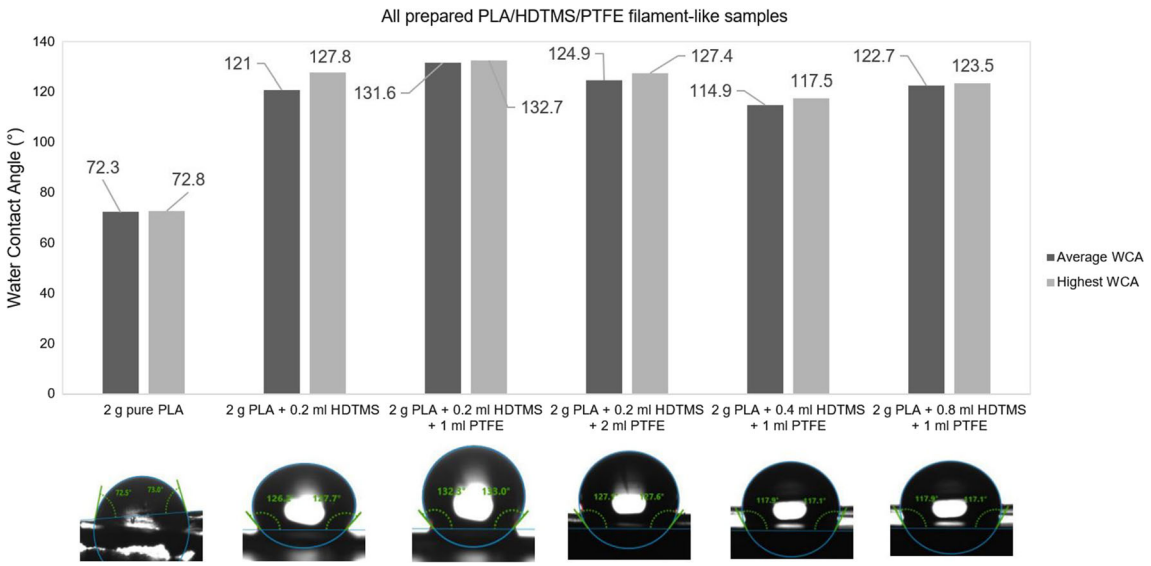

Figure 3 WCA measurements of all prepared PLA/HDTMS/PTFE filaments.

The 2 g pure PLA filament displayed an average WCA of 72.3°, with the highest being 72.8°, clearly indicating that the 2 g of pure PLA filament is hydrophilic. The reason for this hydrophilicity may be the crystals that develop inside the structure due to a slower rate of evaporation, thereby leading to an irregular surface morphology. The 2 g PLA + 0.2 ml HDTMS filament composed of a similar PLA content as the previous sample with an additional 0.2 ml of HDTMS demonstrated an average WCA of 121.0°, with the highest being 127.0°. This confirms that adding HDTMS to PLA increases its hydrophobicity. Similarly, the average WCA of the 2 g PLA + 0.2 ml HDTMS + 2 ml PTFE filament was 124.9°, with the highest recorded as 127.4°, which indicates that increasing the concentration of PTFE did not enhance the hydrophobicity of the PLA/HDTMS/PTFE filaments.

The 2 g PLA + 0.4 ml HDTMS + 1 ml PTFE filament recorded an average WCA of 114.9° with a maximum of 117.5°. Furthermore, the 2 g PLA + 0.8 ml HDTMS + 1 ml PTFE filament containing the same concentrations of PLA and PTFE as the previous sample with 0.8 ml HDTMS displayed an average WCA of 122.7°, while the highest recorded as 123.5°. As shown in Fig. 3, an increase in HDTMS reduced the hydrophobicity of the PLA/HDTMS/PTFE filaments. The HDTMS reflects as a bonding agent to aggregate the silica parties for the HDTMS. Nevertheless, as PTFE volume was increased beyond 1.0 ml, the PLA/HDTMS/PTFE filaments started to degrade after drying, making WCA measurements impossible. Furthermore, due to the increasing amount of PTFE in the PLA/HDTMS/PTFE filaments, when PLA and PTFE are dissolved, the fluorine atoms in PTFE tend to form covalent bonds with the hydrogen atoms in PLA. This is because hydrogen transfers only one electron, while fluorine needs one electron in order to reach a stable state. Therefore, an instant covalent bond is formed when the two elements are combined [51]. Because of this, no fluorine atoms are available to create a fluorine chain above the PLA, thereby deteriorating the surface and decreasing its hydrophobicity.

SEM analysis

Scanning electron microscopy was performed on the 2 g PLA + 0.2 ml HDTMS + 1 ml PTFE filament since it presented the best results. In addition, SEM was used to examine the uniformity of the filaments containing 2 g PLA only and 2 g PLA + 0.2 ml HDTMS to determine how their structures differed from that of the best-performing filament. The SEM analysis was performed on the 2 g PLA + 0.2 ml HDTMS + 1 ml PTFE filaments to observe the uniformity of the reinforcement on the polymeric matrix and to determine the presence of any defects. The solvent was evaporated after drying, and the remaining flat solid material was analyzed. SEM images obtained at various magnifications revealed a uniform distribution of pores with narrow sizes across the entire surface. Figure 4a illustrates the 2 g PLA + 0.2 ml HDTMS + 1 ml PTFE filament's surface at a magnification of 10 μm. It appears that 1 ml of PTFE created an additional layer containing HDTMS on top of the PLA. At this magnification, the surface appears smooth, virtually devoid of peaks and cavities, compared with the same magnification seen on the other filaments.

Additionally, Figs. 4b, c shows a magnified view of the surface of the 2 g PLA + 0.2 ml HDTMS filament at a magnification of 10 μm and 50 μm, respectively. At these magnifications, the images seem to confirm the absence of massive cavities and peaks on the surface. Furthermore, Fig. 4b illustrates the surface at a magnification of 10 μm, which shows the overall smooth structure of the surface. In Fig. 4c, the surface at a magnification of 50 μm illustrates that adding HDTMS to PLA greatly improved its structure by smoothing out its surface and overall reducing the number of cavities. This reduction in the number of cavities and peaks prevents liquid droplets from penetrating the surface, which accounts for the increased hydrophobicity observed in the 2 g PLA + 0.2 ml HDTMS filament. Nevertheless, Figs. 4b, c also exhibits small white spots, which are likely due to the evaporation of solvents during the drying process. The filaments are less voluminous and smaller in size in the case of the 2 g PLA + 0.2 ml HDTMS filament.

Figure 4d shows the surface of a 2 g pure PLA filament at a magnification of 5 μm. The depth of cavities on the surface can be seen at this magnification. In addition, it is clear that a large number of uneven peaks are present on the surface. Figure 4d also shows that pores are generated on the surface of the 2 g pure PLA filament, perhaps due to the formation of pores where microbubbles of chloroform and entrapped air form during the drying process.

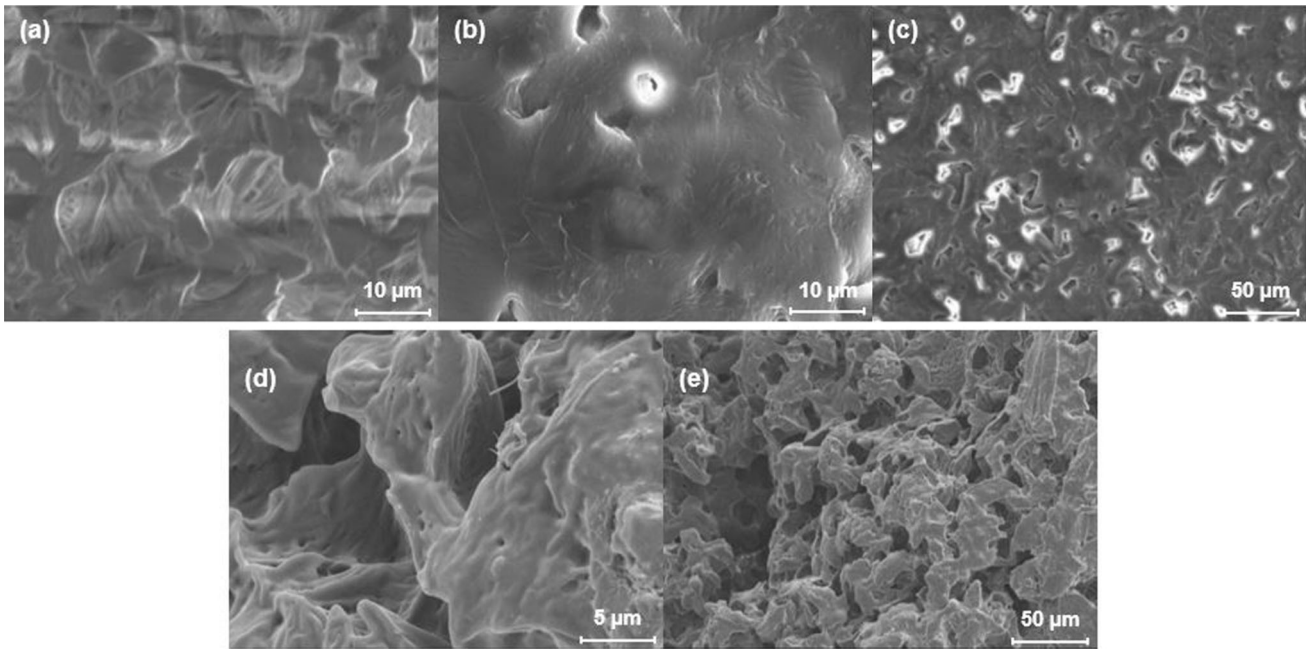

Figure 4 SEM cross-sectional images of filaments: **a** 2 g PLA + 0.2 ml HDTMS + 1 ml PTFE (10 µm); **b** 2 g PLA + 0.2 ml HDTMS (10 µm); **c** 2 g PLA + 0.2 ml HDTMS (50 µm); **d** 2 g pure PLA (5 µm); and **e** 2 g pure PLA (50 µm).

Figure 4e magnifies the 2 g pure PLA filament's surface to a resolution of 50 µm, which shows a homogenous morphology with several peaks and cavities. The many peaks and cavities observed on the surface of the 2 g pure PLA filament allow water droplets to penetrate deeply into these cavities and form a water droplet of a lower Wenzel state, which reduces hydrophobicity [66]. The concentration of a polymer solution is critical to obtaining a viscous solution with a low viscosity, which is also dependent upon the type of polymer used. Therefore, it is possible to incorporate a gradient of concentration between a concentrated polymer solution, its solvent, and air bubbles in the mixture of the polymer solution. The drying process requires a rapid settling of the highly viscous polymer solution at the bottom and rapid migration of the partially diluted polymer solution combined with microbubbles to form pores [8].

FTIR analysis

Functional groups of the PLA/HDTMS/PTFE filaments were identified using Fourier transform infrared spectroscopy. All PLA/HDTMS/PTFE filaments displayed the characteristic bands of PLA. However, when the graphs of both 2 g pure PLA only and 2 g PLA + 0.2 ml HDTMS filaments were analyzed, some similarity in the pattern of peak formation was observed. The structures contain peaks observed at 1043 cm^{-1}, and the peaks formed at 1090 cm^{-1} are a result of C-O bonds. Also, a distinctive band at 1360 cm^{-1} indicates that the hydrogen atom on the phenol group was dissociated. Additionally, the distinctive band observed at 1750 cm^{-1} indicates the carbonyl group's presence from PLA, while the peaks created at 2283 cm^{-1} and 2,950 cm^{-1} were due to the availability of asymmetric $–CH_2$ stretching vibration of the methylene group. Furthermore, the peaks witnessed at 1,452 cm^{-1} and 3000 cm^{-1} were created by aromatic skeletal vibrations combined with methyl and methylene C-H deformations. Nevertheless, the graph of the 2 g PLA + 0.2 ml HDTMS filament-like samples appeared to contain an extra peak at 810 cm-1, which may be ascribed to the stretching and bending vibrations of the Si–O–C bonds (Table 1).

Although the graphs of 2 g pure PLA and 2 g PLA + 0.2 ml HDTMS + 1 ml PTFE filaments were virtually identical, the notable peak can be seen in the graph of the latter at 1655 cm^{-1}, indicating the presence of the carbonyl group from pure PLA. Moreover, the peaks at 2850 cm^{-1} and 2916 cm^{-1} seem to be C-H-stretching modes in the 2 g PLA + 0.2 ml HDTMS + 1 ml PTFE filament. All of this may be

Table 1 FTIR peaks associated with spectra of 2 g PLA + 0.2 ml HDTMS + 1 ml PTFE, 2 g PLA + 0.2 ml HDTMS, and 2 g Pure PLA filaments shown in Fig. 5

Peak number	Wavenumber (cm^{-1})	Vibrational mode
1	810	Si–O–C stretching
2	1043	C–O stretching
3	1090	C–O stretching
4	1360	Symmetric $–CH_3$ bending
5	1452, 3000	Asymmetric $–CH_3$ bending
6	1655	C = O stretching
7	1750	C = O stretching
8	2283, 2950	Asymmetric $–CH_3$ stretching
9	2850, 2915	Asymmetric –CH3 stretching

linked to the presence of CF2 bonds in the 2 g PLA + 0.2 ml HDTMS + 1 ml PTFE filaments. Because pure PLA makes up 10 wt% of the filament, its typical peaks are not strongly exhibited. This has been observed in all of these experimental studies. Overall, the FTIR spectra do not show evidence for the formation of new bonds or moieties, thus demonstrating that no chemical reactions occurred between PLA, HDTMS, and PTFE and that the filament is a true polymer. Figure 5 shows the FTIR spectra of 2 g PLA + 0.2 ml HDTMS + 1 ml PTFE filaments, compared to 2 g pure PLA and 2 g PLA + 0.2 ml HDTMS filaments.

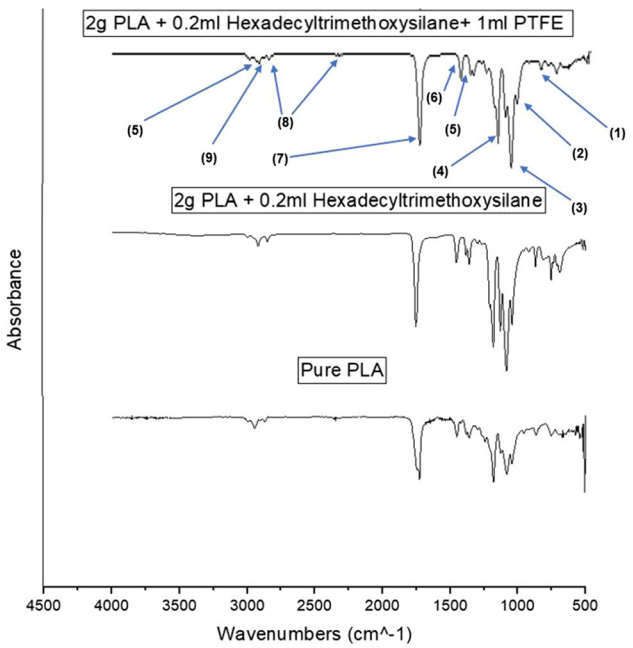

Figure 5 FTIR spectra of filaments: 2 g PLA + 0.2 ml HDTMS + 1 ml PTFE, 2 g PLA + 0.2 ml HDTMS, and 2 g pure PLA. Arrows correspond to peaks detailed in Table 1.

TGA analysis

Thermogravimetric analysis demonstrated that the 2 g PLA + 0.2 ml HDTMS + 1 ml PTFE filament had higher thermal stability than the 2 g pure PLA filament, probably due to PLA hydrolyzing its ester bonds. The mass percent and mass derivative curves were measured to test thermal stability. The degradation temperature, $T_{5\%}$, was determined when the filament lost 5% of its initial mass, and the decomposition temperature, $T_{50\%}$, was derived from the mass derivative curve based on 50% of the initial mass. $T_{5\%}$ and $T_{50\%}$ characterize the temperatures at which 2 g PLA + 0.2 ml HDTMS + 1 ml PTFE filament will degrade and decompose. The development of thermal decomposition largely involves temperature and heating rate.

The TGA curve shown in Fig. 6a was carried out using nitrogen gas at a temperature ranging from 0 °C to 1000 °C, with an increased heating rate of 10 °C/min. According to the graph, thermal decomposition of the sample containing 2 g PLA + 0.2 ml HDTMS + 1 ml PTFE filament commenced at around 100 °C, with 5% of the weight being lost at a temperature ($T_{5\%}$) of approximately 260 °C, which is the same temperature obtained for the 2 g PLA only filament. At 240–360 °C, the 2 g PLA + 0.2 ml HDTMS + 1 ml PTFE filament decomposed swiftly. Moreover, 50% of weight loss was detected at a temperature ($T_{50\%}$) of about 350 °C, and the temperature recorded for the 2 g pure PLA filament. Furthermore, decomposition of the 2 g PLA + 0.2 ml HDTMS + 1 ml PTFE filament takes place starting at a temperature of approximately 250 °C, which is higher than the starting temperature for the 2 g PLA only filament. The move toward higher temperatures in the TGA curves evidently displays that the inclusion of HDTMS and PTFE in PLA impacted its

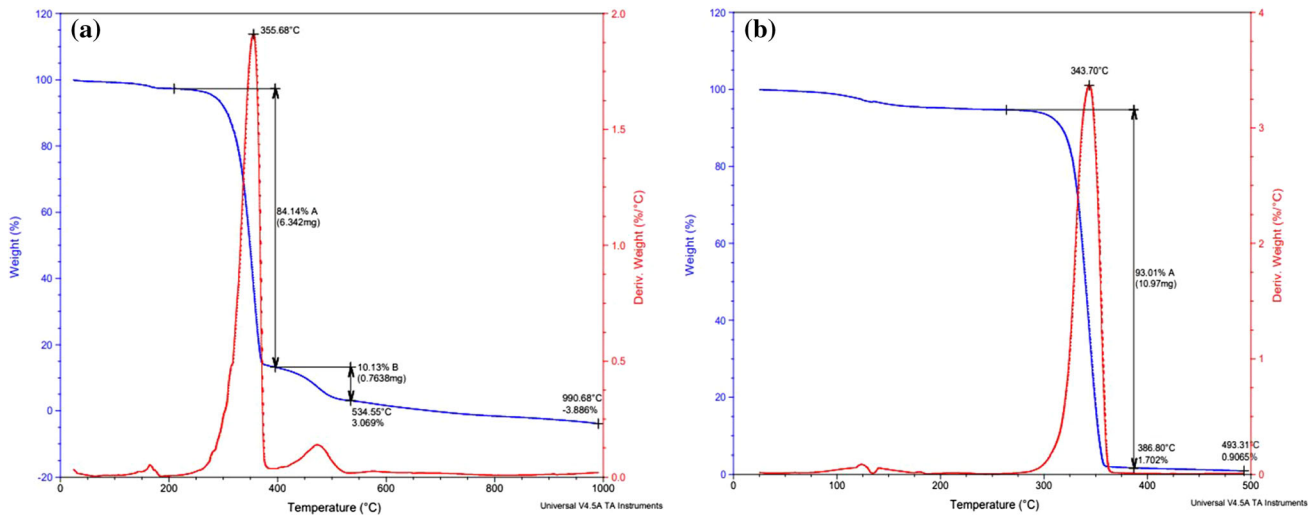

Figure 6 TGA analysis of filaments: **a** 2 g PLA + 0.2 ml HDTMS + 1 ml PTFE, and **b** 2 g pure PLA.

thermal stability. HDTMS and PTFE decompose slower than PLA because of their higher thermal decomposition temperature residual ratios. The decomposition comes to a halt at a temperature of about 370 °C. The 2 g PLA + 0.2 ml HDTMS + 1 ml PTFE filament is heated at a higher rate, the extent of decomposition is less than when 2 g PLA only filament is heated at any given temperature. The rate at which the filament is heated is very vital when considering a case of slow or complex reactions.

The TGA analysis was conducted using nitrogen gas at a temperature ranging from 0 °C to 500 °C, with an increased heating rate of 10 °C/min, to observe the thermal degradation behavior. According to the curve shown in Fig. 6b, for the 2 g pure PLA filament, thermal decomposition commenced at a temperature of approximately 100 °C. Five percent of the weight was lost when the temperature ($T_{5\%}$) reached approximately 260 °C. The loss of weight at $T_{5\%}$ denotes the release of volatiles and water emerging from the PLA hydrolyzing its ester bonds. Additionally, 50% of 2 g pure PLA filament weight loss was observed at a temperature ($T_{50\%}$) of about 340 °C. The TGA curve shows that the decomposition rate peaked around 290 °C, caused by the degradation of PLA molecules during thermal exposure. Finally, decomposition of the 2 g PLA only filament occurred swiftly between 290 °C and 360 °C, with the original 2 g pure PLA filament sample remaining at 360 °C being close to 2 wt%. Last, 2 g pure PLA filament decomposition occurred rapidly between 290 °C and 360 °C, with almost 2 wt% remaining within the original 2 g pure PLA filament at 360 °C. Therefore, the heating rate of the TGA experiments can affect the temperature values for thermal stability. Increasing the heating rate increases thermal stability.

However, unlike the TGA curve for the 2 g only PLA filament, after 370 °C, decomposition of the 2 g PLA + 0.2 ml HDTMS + 1 ml PTFE filament is not uniform. The weight percentage of the original 2 g PLA + 0.2 ml HDTMS + 1 ml PTFE filament remaining observed at around 370 °C was about 12wt%, which was far greater than the weight remaining for the 2 g pure PLA filament at an almost similar temperature. Furthermore, 2% of the original 2 g PLA + 0.2 ml HDTMS + 1 ml PTFE filament's weight remaining was recorded at ~ 535 °C, which exceeded the temperature recorded for the 2% weight remaining of the 2 g pure PLA filament. When decomposition curves shifted to higher temperatures as heating rate increased, decomposition occurred over a larger temperature range, and the corresponding decomposition curves broadened. According to the data obtained, it was confirmed that the inclusion of HDTMS and PTFE in PLA substantially increased PLA's thermal resistance in the 2 g PLA + 0.2 ml HDTMS + 1 ml PTFE filament. This might reflect higher mechanical properties for advanced AM purposes.

Conclusion

In this study, HDTMS and PTFE were dispersed in a PLA thermoplastic using solvent casting and melt extrusion to produce a hydrophobic PLA/HDTMS/PTFE filament that could be used for the FFF AM process. It was discovered that the filament prepared with an inclusion of 0.2 ml HDTMS and 1 ml PTFE to 2 g PLA of solution greatly increased its hydrophobicity, and a WCA of 132.7° was observed. In addition, several characterization tests were conducted to determine how the PLA/HDTMS/PTFE filaments behaved structurally. According to SEM results, only 2 g PLA had a porous surface with many cavities and peaks, which resulted in low hydrophobicity. However, it was discovered that adding 0.2 ml HDTMS and 1 ml PTFE to 2 g PLA created an additional layer of PTFE above the existing surface, which increased its hydrophobicity. FTIR spectra of the 2 g PLA + 0.2 ml HDTMS + 1 ml PTFE filament confirmed the presence of PLA, PTFE, and HDTMS. Compared with 2 g pure PLA filament, the 2 g PLA + 0.2 ml HDTMS + 1 ml PTFE filament exhibited superior thermal properties, indicating the ease with which PLA/HDTMS/PTFE filaments can be used in FFF. As a result of this study, a promising area for the future development of PLA filament fabrication with various polymers is open for a wide range of industrial applications.

References

[1] Avramescu RE, Ghica MV, Dinu-Pîrvu C, Prisada R, Popa L (2018) Superhydrophobic natural and artificial Surfaces—A structural approach. Materials (Basel) 11:866. https://doi.org/10.3390/ma11050866

[2] Parvate S, Dixit P, Chattopadhyay S (2020) Superhydrophobic Surfaces: insights from Theory and Experiment. J Phys Chem B 124:1323–1360. https://doi.org/10.1021/acs.jpcb.9b08567

[3] Shahzadi P, Gilani SR, Rana BB, Ghaffar A, Munir A (2021) Transparent, self-cleaning, scratch resistance and environment friendly coatings for glass substrate and their potential applications in outdoor and automobile industry. Sci Rep 11:1–14. https://doi.org/10.1038/s41598-021-00230-9

[4] Ng YH, Tay SW, Hong L (2018) Formation of icephobic surface with micron-scaled hydrophobic heterogeneity on polyurethane aerospace coating. ACS Appl Mater Interfaces 10:37517–37528. https://doi.org/10.1021/acsami.8b13403

[5] Tran PA, Hocking DM, O'Connor AJ (2015) In situ formation of antimicrobial silver nanoparticles and the impregnation of hydrophobic polycaprolactone matrix for antimicrobial medical device applications. Mater Sci Eng C 47:63–69. https://doi.org/10.1016/j.msec.2014.11.016

[6] A. Gapeeva, I. Hölken, R. Adelung, M. Baum, (2017) Characterization of a polydimethylsiloxane-polythiourethane polymer blend with potential as fouling-release coating, In: Proceedings 2017 IEEE 7th International Conference Nanomaterials: Application & Properties: pp. 01FNC08–1

[7] Milles S, Soldera M, Voisiat B, Lasagni AF (2019) Fabrication of superhydrophobic and ice-repellent surfaces on pure aluminium using single and multiscaled periodic textures. Sci Rep 9:1–13. https://doi.org/10.1038/s41598-019-49615-x

[8] Hossain KMZ, Felfel RM, Ogbilikana PS, Thakker D, Grant DM, Scotchford CA, Ahmed I (2018) Single solvent-based film casting method for the production of porous polymer films. Macromol Mater Eng 303:1700628. https://doi.org/10.1002/mame.201700628

[9] SlepickovaKasalkova N, Slepicka P, Kolska Z, Svorcik V (2015) Wettability and Other Surface Properties of Modified Polymers. In: Aliofkhazraei M (ed) Wetting and Wettability. InTech, London, pp 323–356

[10] Dai X, Stogin BB, Yang S, Wong TS (2015) Slippery Wenzel State. ACS Nano 9:9260–9267. https://doi.org/10.1021/acsnano.5b04151

[11] Lu Y (2017) Fabrication of a lotus leaf-like hierarchical structure to induce an air lubricant for drag reduction. Surf Coatings Technol 331:48–56. https://doi.org/10.1016/j.surfcoat.2017.10.001

[12] Zhi J, Zhang LZ (2017) Durable superhydrophobic surfaces made by intensely connecting a bipolar top layer to the substrate with a middle connecting layer. Sci Rep 7:1–12. https://doi.org/10.1038/s41598-017-10030-9

[13] Di Mundo R, Palumbo F, D'Agostino R (2010) Influence of chemistry on wetting dynamics of nanotextured hydrophobic surfaces. Langmuir 26:5196–5201. https://doi.org/10.1021/la903654n

[14] Darmanin T, De Givenchy ET, Amigoni S, Guittard F (2013) Superhydrophobic surfaces by electrochemical processes. Adv Mater 25:1378–1394. https://doi.org/10.1002/adma.201204300

[15] Di Mundo R, Labianca C, Carbone G, Notarnicola M (2020) Recent advances in hydrophobic and icephobic surface treatments of concrete. Coatings 10:449. https://doi.org/10.3390/COATINGS10050449

[16] Walunj A, Sathyabhama A (2018) Influence of surface roughness on pool boiling heat transfer. IOP Conf Ser Mater Sci Eng 402:802–811. https://doi.org/10.1088/1757-899X/402/1/012081

[17] Dong F, Padua GW, Wang Y (2013) Controlled formation of hydrophobic surfaces by self-assembly of an amphiphilic natural protein from aqueous solutions. Soft Matter 9:5933–5941. https://doi.org/10.1039/c3sm50667c

[18] Bormashenko E, Chaniel G, Gendelman O (2014) Hydrophilization and hydrophobic recovery in polymers obtained by casting of polymer solutions on water surface. J Colloid Interface Sci 435:192–197. https://doi.org/10.1016/j.jcis.2014.06.053

[19] Mahadik SA, Mahadik SS (2021) Surface morphological and topographical analysis of multifunctional superhydrophobic sol-gel coatings. Ceram Int 47:29475–29482. https://doi.org/10.1016/j.ceramint.2021.07.115

[20] Tomšík E, Dallas P, Šeděnková I, Svoboda J, Hrubý M (2021) Electrochemical deposition of highly hydrophobic perfluorinated polyaniline film for biosensor applications. RSC Adv 11:18852–18859. https://doi.org/10.1039/d1ra02325j

[21] Moghadasi H, Fathalizadeh H, Mehdikhani A, Saffari H (2021) (2021) Surface modification utilizing photolithography process for pool boiling enhancement: an experimental study. Heat Transf Eng. https://doi.org/10.1080/014576321932037

[22] Saleh TA, Baig N (2019) Efficient chemical etching procedure for the generation of superhydrophobic surfaces for separation of oil from water. Prog Org Coatings 133:27–32. https://doi.org/10.1016/j.porgcoat.2019.03.049

[23] He X, Liang C, Liu Q, Xu Z (2019) Magnetically responsive Janus nanoparticles synthesized using cellulosic materials for enhanced phase separation in oily wastewaters and water-in-crude oil emulsions. Chem Eng J 378:122045. https://doi.org/10.1016/j.cej.2019.122045

[24] Foster W, Miyazawa K, Fukuma T, Kusumaatmaja H, Voïtchovsky K (2020) Self-assembly of small molecules at hydrophobic interfaces using group effect. Nanoscale 12:5452–5463. https://doi.org/10.1039/c9nr09505e

[25] Amudha A, Shashikala HD, Asiq Rahman OS, Keshri AK, Nagaraja HS (2019) Effect of graphene oxide loading on plasma sprayed alumina-graphene oxide composites for improved anticorrosive and hydrophobic surface. Surf Topogr Metrol Prop 7:24003. https://doi.org/10.1088/2051-672X/ab2707

[26] Magisetty RP, Shukla A, Kandasubramanian B (2018) Dielectric, hydrophobic investigation of ABS/NiFe2O4 nanocomposites fabricated by atomized spray assisted and solution casted techniques for miniaturized electronic applications. J Electron Mater 47:5640–5656. https://doi.org/10.1007/s11664-018-6452-x

[27] Colson P, Henrist C, Cloots R (2013) Nanosphere lithography: a powerful method for the controlled manufacturing of nanomaterials. J Nanomater. https://doi.org/10.1155/2013/948510

[28] Refino AD, Yulianto N, Syamsu I, Nugroho AP, Hawari NH, Syring A, Kartini E, Iskandar F, Voss T, Sumboja A, Peiner E, Wasisto HS (2021) Versatilely tuned vertical silicon nanowire arrays by cryogenic reactive ion etching as a lithium-ion battery anode. Sci Rep 11:1–15. https://doi.org/10.1038/s41598-021-99173-4

[29] Tan XM, Rodrigue D (2019) A review on porous polymeric membrane preparation. Part II: production techniques with polyethylene, polydimethylsiloxane, polypropylene, polyimide, and polytetrafluoroethylene. Polymers (Basel). https://doi.org/10.3390/polym11081310

[30] Guo X, Liu L, Zhuang Z, Chen X, Ni M, Li Y, Cui Y, Zhan P, Yuan C, Ge H, Wang Z, Chen Y (2015) A new strategy of lithography based on phase separation of polymer blends. Sci Rep 5:1–12. https://doi.org/10.1038/srep15947

[31] Zhao S, Zhang G, Shen W, Wang X, Liu F (2020) Design and fabrication of highly selective and permeable polymer membranes. J Appl Phys 128:131102. https://doi.org/10.1063/5.0015975

[32] Carbone EAD, Boucher N, Sferrazza M, Reniers F (2010) How to increase the hydrophobicity of PTFE surfaces using an r.f. atmospheric-pressure plasma torch. Surf Interface Anal 42:1014–1018. https://doi.org/10.1002/sia.3384

[33] Ryu YS, Kim IS, Kim SH (2019) Effect of modified ZnO nanoparticle on the properties of polylactide ultrafine fibers. J Appl Polym Sci 136:47446. https://doi.org/10.1002/app.47446

[34] Shaker M, Salahinejad E, Ashtari-Mahini F (2018) Hydrophobization of metallic surfaces by means of Al 2 O 3 -HDTMS coatings. Appl Surf Sci 428:455–462. https://doi.org/10.1016/j.apsusc.2017.09.184

[35] Chua MH, Cheng W, Goh SS, Kong J, Li B, Lim JYC, Mao L, Wang S, Xue K, Yang L, Ye E, Zhang K, Cheong WCD, Tan BH, Li Z, Tan BH, Loh XJ (2020) Face masks in the new COVID-19 normal: materials testing, and perspectives. Research. https://doi.org/10.34133/2020/7286735

[36] Patel V, Chesmore A, Legner CM, Pandey S (2022) Trends in workplace wearable technologies and connected-worker solutions for next-generation occupational safety, health, and productivity. Adv Intell Syst 4:2100099. https://doi.org/10.1002/aisy.202100099

[37] Ligon SC, Liska R, Stampfl J, Gurr M, Mülhaupt R (2017) Polymers for 3D printing and customized additive

manufacturing. Chem Rev 117:10212–10290. https://doi.org/10.1021/acs.chemrev.7b00074

[38] Zhai Y, Lados DA, Lagoy JL (2014) Additive Manufacturing: making imagination the major limitation. Jom 66:808–816. https://doi.org/10.1007/s11837-014-0886-2

[39] Tofail SAM, Koumoulos EP, Bandyopadhyay A, Bose S, O'Donoghue L, Charitidis C (2018) Additive manufacturing: scientific and technological challenges, market uptake and opportunities. Mater Today 21:22–37. https://doi.org/10.1016/j.mattod.2017.07.001

[40] Abudula T, Qurban RO, Bolarinwa SO, Mirza AA, Pasovic M, Memic A (2020) 3D Printing of metal/metal oxide incorporated thermoplastic nanocomposites with antimicrobial properties. Front Bioeng Biotechnol 8:1046. https://doi.org/10.3389/fbioe.2020.568186

[41] Yusuf SM, Cutler S, Gao N (2019) Review: the impact of metal additive manufacturing on the aerospace industry. Metals (Basel) 9:1286. https://doi.org/10.3390/met9121286

[42] Sinha R, Sanchez A, Camara-Torres M, Uriszar-Aldaca IC, Calore AR, Harings J, Gambardella A, Ciccarelli L, Vanzanella V, Sisani M, Scatto M, Wendelbo R, Perez S, Villanueva S, Matanza A, Patelli A, Grizzuti N, Mota C, Moroni L (2021) Additive manufactured scaffolds for bone tissue engineering: physical characterization of thermoplastic composites with functional fillers. ACS Appl Polym Mater 3:3788–3799. https://doi.org/10.1021/acsapm.1c00363

[43] Alghamdi SS, John S, Choudhury NR, Dutta NK (2021) Additive manufacturing of polymer materials: progress, promise and challenges. Polymers (Basel) 13:1–39. https://doi.org/10.3390/polym13050753

[44] Razavykia A, Brusa E, Delprete C, Yavari R (2020) An overview of additive manufacturing technologies—A review to technical synthesis in numerical study of selective laser melting. Materials (Basel) 13:3895. https://doi.org/10.3390/ma13173895

[45] Singh R, Gupta A, Tripathi O, Srivastava S, Singh B, Awasthi A, Rajput SK, Sonia P, Singhal P, Saxena KK (2019) Powder bed fusion process in additive manufacturing: an overview. Mater Today Proc 26:3058–3070. https://doi.org/10.1016/j.matpr.2020.02.635

[46] Huang J, Qin Q, Wang J (2020) A review of stereolithography: processes and systems. Processes 8:1138. https://doi.org/10.3390/PR8091138

[47] Gülcan O, Günaydın K, Tamer A (2021) The state of the art of material jetting—A critical review. Polymers (Basel). https://doi.org/10.3390/polym13162829

[48] Pérez-Castillo JL, Cuan-Urquizo E, Roman-Flores A, Olvera-Silva O, Romero-Muñoz V, Gómez-Espinosa A, Ahmad R (2021) Curved layered fused filament fabrication: an overview. Addit Manuf 47:102354. https://doi.org/10.1016/j.addma.2021.102354

[49] Aydin A, Demirtas Z, Ok M, Erkus H, Cebi G, Uysal E, Gunduz O, Ustundag CB (2021) 3D printing in the battle against COVID-19. Emergent Mater 4:363–386. https://doi.org/10.1007/s42247-021-00164-y

[50] Fonseca AC, Melchels FPW, Ferreira MJS, Moxon SR, Potjewyd G, Dargaville TR, Kimber SJ, Domingos M (2020) Emulating human tissues and organs: a bioprinting perspective toward personalized medicine. Chem Rev 120:11128–11174. https://doi.org/10.1021/acs.chemrev.0c00342

[51] Puts GJ, Crouse P, Ameduri BM (2019) Polytetrafluoroethylene: synthesis and characterization of the original extreme polymer. Chem Rev 119:1763–1805. https://doi.org/10.1021/acs.chemrev.8b00458

[52] Subeshan B, Alonayni A, Rahman MM, Asmatulu E (2018) Investigating compression strengths of 3D printed polymeric infill specimens of various geometries. Int Soc Opt Eng. https://doi.org/10.1117/12.2296651

[53] Rane R, Kulkarni A, Prajapati H, Taylor R, Jain A, Chen V (2020) Post-process effects of isothermal annealing and initially applied static uniaxial loading on the ultimate tensile strength of fused filament fabrication parts. Materials (Basel) 13:352. https://doi.org/10.3390/ma13020352

[54] Pranzo D, Larizza P, Filippini D, Percoco G (2018) Extrusion-based 3D printing of microfluidic devices for chemical and biomedical applications: a topical review. Micromachines 9:374. https://doi.org/10.3390/mi9080374

[55] Angelopoulos PM, Samouhos M, Taxiarchou M (2019) Functional fillers in composite filaments for fused filament fabrication: a review. Mater Today Proc 37:4031–4043. https://doi.org/10.1016/j.matpr.2020.07.069

[56] Brounstein Z, Yeager CM, Labouriau A (2021) Development of antimicrobial PLA composites for fused filament fabrication. Polymers (Basel) 13:1–18. https://doi.org/10.3390/polym13040580

[57] Gusain A, Thankappan A, Thomas S (2020) Roll-to-roll printing of polymer and perovskite solar cells: compatible materials and processes. J Mater Sci 55:13490–13542. https://doi.org/10.1007/s10853-020-04883-1

[58] Toh HW, Toong DWY, Ng JCK, Ow V, Lu S, Tan LP, Wong PEH, Venkatraman S, Huang Y, Ang HY (2021) Polymer blends and polymer composites for cardiovascular implants. Eur Polym J 146:110249. https://doi.org/10.1016/j.eurpolymj.2020.110249

[59] Wang J, Gao H, Hu Y, Zhang N, Zhou W, Wang C, Binks BP, Yang Z (2021) 3D printing of Pickering emulsion inks to construct poly(D, L-lactide-co-trimethylene carbonate)-based porous bioactive scaffolds with shape memory effect.

J Mater Sci 56:731–745. https://doi.org/10.1007/s10853-020-05318-7

[60] Vaes D, Van Puyvelde P (2021) Semi-crystalline feedstock for filament-based 3D printing of polymers. Prog Polym Sci 118:101411. https://doi.org/10.1016/j.progpolymsci.2021.101411

[61] Singh S, Singh G, Prakash C, Ramakrishna S (2020) Current status and future directions of fused filament fabrication. J Manuf Process 55:288–306. https://doi.org/10.1016/j.jmapro.2020.04.049

[62] Dey A, Eagle INR, Yodo N (2021) A review on filament materials for fused filament fabrication. J Manuf Mater Process 5:69. https://doi.org/10.3390/jmmp5030069

[63] Gama N, Ferreira A, Barros-Timmons A, Evtuguin D (2021) Polyamide 6/modified pine bark particle composites for additive manufacturing. J Mater Sci 56:19093–19105. https://doi.org/10.1007/s10853-021-06443-7

[64] Saha PK, Mia R, Zhou Y, Ahmed T (2021) Functionalization of hydrophobic nonwoven cotton fabric for oil and water repellency. SN Appl Sci 3:1–18. https://doi.org/10.1007/s42452-021-04582-9

[65] Schroepfer M, Junghans F, Voigt D, Meyer M, Breier A, Schulze-Tanzil G, Prade I (2020) Gas-phase fluorination on PLA improves cell adhesion and spreading. ACS Appl Mater Interfaces 5:5498–5507. https://doi.org/10.1021/acsomega.0c00126

[66] He B, Patankar NA, Lee J (2003) Multiple equilibrium droplet shapes and design criterion for rough hydrophobic surfaces. Langmuir 19:4999–5003. https://doi.org/10.1021/la0268348